

UCLA

UCLA Previously Published Works

Title

Default Mode Network quantitative diffusion and resting-state functional magnetic resonance imaging correlates in sporadic Creutzfeldt-Jakob disease

Permalink

<https://escholarship.org/uc/item/8qc4f562>

Journal

Human Brain Mapping, 43(13)

ISSN

1065-9471

Authors

Paoletti, Matteo
Caverzasi, Eduardo
Mandelli, Maria Luisa
[et al.](#)

Publication Date

2022-09-01

DOI

10.1002/hbm.25945










Copyright Information

This work is made available under the terms of a Creative Commons Attribution-NonCommercial License, available at <https://creativecommons.org/licenses/by-nc/4.0/>

Peer reviewed

RESEARCH ARTICLE

Default Mode Network quantitative diffusion and resting-state functional magnetic resonance imaging correlates in sporadic Creutzfeldt-Jakob disease

Matteo Paoletti^{1,2}  | Eduardo Caverzasi^{3,4}  | Maria Luisa Mandelli¹  |
 Jesse A. Brown¹  | Roland G. Henry^{3,5,6}  | Bruce L. Miller¹  |
 Howard J. Rosen¹  | Stephen J. DeArmond⁷ | Stefano Bastianello^{2,4} |
 William W. Seeley^{1,7}  | Michael D. Geschwind¹ 

¹Memory and Aging Center, Department of Neurology, Weill Institute for Neuroscience, University of California San Francisco, San Francisco, California, USA

²Department of Neuroradiology, IRCCS Mondino Foundation, Pavia, Italy

³Weill Institute for Neurosciences, Department of Neurology, University of California San Francisco, San Francisco, California, USA

⁴Department of Brain and Behavioral Sciences, University of Pavia, Pavia, Italy

⁵Graduate Group in Bioengineering, University of California San Francisco, San Francisco, California, USA

⁶Department of Radiology and Biomedical Imaging, University of California San Francisco, San Francisco, California, USA

⁷Department of Pathology, University of California, San Francisco, California, USA

Correspondence

Eduardo Caverzasi, Weill Institute for Neurosciences, Department of Neurology, University of California San Francisco, 675 Nelson Rising Lane, San Francisco, CA 94158, USA.
 Email: eduardo.caverzasi@ucsf.edu

Funding information

Larry L. Hillblom Foundation Hellman Family Foundation; Michael J. Homer Family Fund; National Institutes of Health (NIH), Grant/Award Numbers: R01 AG031189, R56AG055619, R01AG062562, P30AG062422, UL1RR024131, UL1TR000004, R01AG032289

Abstract

Grey matter involvement is a well-known feature in sporadic Creutzfeldt–Jakob disease (sCJD), yet precise anatomy-based quantification of reduced diffusivity is still not fully understood. Default Mode Network (DMN) areas have been recently demonstrated as selectively involved in sCJD, and functional connectivity has never been investigated in prion diseases. We analyzed the grey matter involvement using a quantitatively multi-parametric MRI approach. Specifically, grey matter mean diffusivity of 37 subjects with sCJD was compared with that of 30 age-matched healthy controls with a group-wise approach. Differences in mean diffusivity were also examined between the cortical (MM(V)1, MM(V)2C, and VV1) and subcortical (VV2 and MV2K) subgroups of sCJD for those with autopsy data available ($n = 27$, 73%). We also assessed resting-state functional connectivity of both ventral and dorsal components of DMN in a subset of subject with a rs-fMRI dataset available ($n = 17$). Decreased diffusivity was predominantly present in posterior cortical regions of the DMN, but also outside of the DMN in temporal areas and in a few limbic and frontal areas, in addition to extensive deep nuclei involvement. Both subcortical and cortical sCJD

Abbreviations: ADC, apparent diffusion coefficient; dDMN, dorsal DMN; DMN, Default Mode Network; DTI, diffusion tensor imaging; DWI, diffusion-weighted imaging; FLAIR, fluid-attenuated inversion recovery; GM, grey matter; GP, globus pallidus; HARDI, high angular resolution diffusion-weighted imaging; MD, mean diffusivity; MMSE, Mini-Mental State Examination; MNI, Montreal Neurological Institute; PCC, posterior cingulate cortex; PRNP, prion protein gene; rs-fMRI, resting-state functional MRI; sCJD, sporadic Creutzfeldt–Jakob disease; UCSF, University of California San Francisco; vDMN, ventral DMN; VOI, volume of interest.

Matteo Paoletti and Eduardo Caverzasi contributed equally to this work.

This is an open access article under the terms of the [Creative Commons Attribution-NonCommercial](https://creativecommons.org/licenses/by-nc/4.0/) License, which permits use, distribution and reproduction in any medium, provided the original work is properly cited and is not used for commercial purposes.

© 2022 The Authors. *Human Brain Mapping* published by Wiley Periodicals LLC.

subgroups showed decreased diffusivity subcortically, whereas only the cortical type expressed significantly decreased diffusivity cortically, mainly in parietal, occipital, and medial-inferior temporal cortices bilaterally. Interestingly, we found abnormally increased connectivity in both dorsal and ventral components of the DMN in sCJD subjects compared with healthy controls. The significance and possible utility of functional imaging as a biomarker for tracking disease progression in prion disease needs to be explored further.

KEYWORDS

CJD, DMN, fMRI, MD, mean diffusivity, MRI, resting-state, sporadic Jakob–Creutzfeldt disease

1 | INTRODUCTION

Sporadic Creutzfeldt–Jakob disease (sCJD) is the most common human prion disease, a group of rare diseases due to misfolding of the normal prion protein, which results in neurodegeneration. The disease is typically characterized by rapidly progressive dementia, ataxia, and myoclonus progressing to death usually within a year or less from onset (Brown et al., 1986), but presentations can be quite heterogeneous (Collins et al., 2006; Geschwind, 2015; Parchi et al., 1999). Diffusion-weighted imaging (DWI) brain MRI shows a pattern of decreased diffusivity with high diagnostic sensitivity and specificity and has consequently been included in updated sCJD diagnostic criteria (Bizzi et al., 2020; Geschwind et al., 2007; Staffaroni et al., 2017; Vitali et al., 2011; WHO, 1998; Zerr et al., 2009).

Most imaging studies in sCJD have evaluated signal abnormalities on fluid-attenuated inversion recovery (FLAIR) and especially DWI by visual assessment (Eisenmenger et al., 2015; Kallenberg et al., 2006; Meissner et al., 2009; Shiga et al., 2004; Tschampa et al., 2007; Vitali et al., 2011; Young et al., 2005; Zerr et al., 2009). These diffusivity changes in sCJD have been associated mainly with vacuolation (Figini et al., 2015; Geschwind et al., 2009; Manners et al., 2009).

Qualitative visual assessment of reduced diffusivity on DWI images is very helpful for sCJD diagnosis (Hermann et al., 2021; Zerr et al., 2009), but has several shortcomings due to the subjectivity of readings and difficulty distinguishing true abnormalities from artifact, and therefore may increase the risk of under- or over-estimating the real extent of disease involvement (Caverzasi, Henry, et al., 2014; Lin et al., 2006). To overcome such limitations, quantitative approaches have been used to more precisely assess diffusivity metrics, especially mean diffusivity (MD), in prion diseases (Caverzasi, Henry, et al., 2014; Caverzasi, Mandelli, et al., 2014; Eisenmenger et al., 2015; Grau-Rivera et al., 2017; Manners et al., 2009; Ukisu et al., 2005; Wang et al., 2013). A quantitative approach, in fact, may be more precise at determining involved regions and investigating the heterogeneity of radiological patterns of abnormalities (Grau-Rivera et al., 2017; 2014; Sacco et al., 2020).

Visual and quantitative assessments of diffusivity abnormalities in sCJD, although heterogeneous, generally show prominent involvement of the anterior cingulate, parieto-angular, retrosplenial, and middle temporal cortices (Caverzasi, Henry, et al., 2014; Vitali et al., 2011) areas that

are part of the Default Mode Network (DMN) (Alves et al., 2019; Buckner et al., 2008; Leech & Sharp, 2014). In a recent voxel-based morphometry study, we found selective atrophy in almost all regions part of DMN, further suggesting that DMN network could be a preferential site of involvement in prion disease (Younes et al., 2021).

To our knowledge, functional connectivity has not been investigated in prion disease, yet analysis of resting-state functional MRI (rs-fMRI) can have a role in identifying dysfunction before structural and possibly even diffusivity abnormalities may be identified. In non-prion neurodegenerative diseases, a correlation between the pattern of involvement (usually by atrophy) and dysfunction of intrinsic connectivity networks is often seen (Gardner et al., 2013; Seeley et al., 2009; Zhou et al., 2010), and functional measures have also been shown to be sensitive to disease involvement even in regions without suspected or measured atrophy (Dopper et al., 2013; Hacker et al., 2012; Nestor et al., 2018).

In the present work, we aimed (a) to assess quantitatively the diffusivity abnormalities in sCJD grey matter to demonstrate preferential involvement of the DMN-related areas; (b) to investigate if patterns of involvement specific for sCJD molecular subtypes might be detected by quantitative analysis; and (c) to investigate any resting-state functional abnormality within the DMN in sCJD.

2 | MATERIALS AND METHODS

2.1 | Subjects

From June 2008 to September 2015, 64 subjects with rapidly progressive dementia ultimately diagnosed by us with probable and/or definite sCJD had a research visit at our center at the University of California San Francisco (UCSF) Memory and Aging Center (MAC). All met UCSF 2007 probable or definite sporadic CJD criteria (Geschwind et al., 2007; Kretschmar et al., 1996; Parchi et al., 1999) (many also eventually met either WHO 1998 or European probable sCJD criteria (WHO, 1998; Zerr et al., 2009)). 58 subjects had a 3T MRI (Siemens Trio Syngo), but only 49 had the same high angular resolution diffusion-weighted imaging (HARDI) acquisition for diffusion tensor imaging (DTI) analysis. Twelve subject's scans were excluded because of poor quality images due to severe motion artifact. Thus, 37 subjects were included in the diffusion dataset of this study (mean

age 64 ± 7.8 , 17 females). The same sCJD cohort has been recently presented in another paper from our group (Sacco et al., 2020). A rs-fMRI acquisition was added to the protocol in mid-2011 and acquired in a subgroup of subjects ($n = 19$). Of those nineteen, two were excluded for head motion, based on a threshold of >3 mm translational movement or $>3^\circ$ relative rotation or number of motion spikes $>10\%$ of the total (relative motion >1 mm), leaving 17 subjects used in the functional analysis.

Genotyping for pathogenic prion protein gene (*PRNP*) mutations and codon 129 polymorphisms were performed through the U.S. National Prion Disease Pathology Surveillance Center (NPDPS; Cleveland, OH). *PRNP* genotype and codon 129 polymorphism data were available in all 37 subjects; none had mutations. Twenty-seven subjects (73%) were pathologically proven, all of whom had prion typing (Kretschmar et al., 1996; Parchi et al., 1999).

A detailed standardized neurological examination and testing, including Mini-Mental State Examination (MMSE) and modified Barthel index (Mahoney & Barthel, 1965), were recorded ± 3 days from MRI date.

Thirty healthy age and sex-matched subjects who underwent the same MRI protocol on the same scanner were selected from the MAC database (mean age 63.4 ± 10.5 SD, 15 females) as controls. Participants or their caregivers provided informed consent to the present study, which was approved by the UCSF Committee on Human Research.

2.2 | MRI acquisition

The HARDI dataset was acquired using a single-shot spin-echo echo-planar imaging (EPI) sequence including 55 contiguous axial slices acquired in an interleaved order (TR/TE = 8000/109 ms; flip angle = 90° ; matrix = 100×100 ; in-plane resolution = 2.2 mm^2 ; slice thickness = 2.2 mm; 64 noncollinear diffusion sensitization directions at $b = 2000 \text{ s/mm}^2$, 1 at $b = 0$; integrated parallel acquisition technique acceleration (IPAT) factor = 2).

For functional imaging, 36 interleaved axial slices (slice thickness = 3 mm with 0.6 mm gap) were acquired using a T_2^* -weighted EPI sequence (TR/TE = 2000/27 ms, flip angle = 80° ; field of view = $230 \times 230 \text{ mm}^2$; matrix = 92×92 ; in-plane resolution = $2.5 \times 2.5 \text{ mm}$; 240 volumes) with an online gradient adjustment for head motion compensation. Participants were instructed to lie still with their eyes closed, and to remain awake, thinking of nothing.

A T1-weighted (T1w) sequence was acquired for all subjects for structural reference and for purpose of registration.

2.3 | Image processing and analysis

2.3.1 | Diffusion imaging

Preprocessing

Initial image preprocessing was performed using the FMRIB Software Library (FSL; <http://www.fmrib.ox.ac.uk/fsl/>). FSL's brain extraction

tool was used for skull stripping. Preprocessing of HARDI datasets was performed using FSL's diffusion toolbox. Eddy current distortions and motion artifacts were corrected by registering each diffusion-sensitized volume to the b_0 volume with an affine transform. After tensor diagonalization, whole-brain maps of voxel-wise quantitative DTI metrics were obtained, most importantly for this paper, MD. For each subject, the b_0 volume of the DWI dataset was registered to T1w image through dedicated boundary-based registration (BBR) (Greve & Fischl, 2009). The T1w image was registered to the Montreal Neurological Institute (MNI) standard atlas using FSL's linear and nonlinear registration tool. MD maps were warped to MNI space using the transform estimated for the registration of T1w image to MNI space.

Group-wise analysis

For both subjects and controls, the average MD was determined for each brain GM region (cortical, subcortical and cerebellum) and for each of 41 GM volume-of-interest (VOI) per hemisphere (Desikan et al., 2006; Fischl et al., 2002). To decrease the potential effect of partial volume artifact, a threshold intensity (average intensity of CSF extracted in ventricles -2 SD, [0.0016–0.00023]) was used to exclude voxels that were likely to contain a mixture of CSF with GM from the VOI boundary. We considered caudate, putamen, globus pallidus (GP), and thalami as subcortical VOIs. For all analyses, FDR correction for multiple comparisons was applied: significance was set at $p < .05$ FDR corrected. As post hoc analysis, we also built single-subject MD-based involvement maps on the MNI space to explore the feasibility of such an approach and to corroborate the group-wise analysis (see Supporting Information).

Sub-group analysis by cortical or subcortical major involvement

Given the molecular subdivision of our cohort (see Table 1) we did not have enough subjects to conduct a MD analysis relative to each pure subtype (e.g., MM1, VV1 etc.). Following previous publications by other groups, we subdivided our sCJD cohort of pathology-proven cases in two different subgroups based on molecular classification: a cortical-predominant subtype, "cortical subgroup," (including MM(V)1, MM(V)2C, and VV1 subtypes) and a subcortical-predominant subtype, "subcortical subgroup" (including VV2 and MV2K subtypes) (Bizzi et al., 2021; Pascuzzo et al., 2020). The molecular classification needed for such a division was available for 27 of the 37 cases. Subjects with the coexistence of multiple molecular subtypes (e.g., MMV1-2, MMV2K+2C, etc.) which would have a mixture of cortical and subcortical types, however, were excluded from this subgroup analysis, resulting in 19 cortical sCJD subjects (1 MM1, 1 VV1, 2 MM1-2C, 7 MM2C, 4 MV1, 4 MV2C) and 5 subcortical sCJD subjects (2 MV2K, 3 VV2).

Statistics

Age-corrected z-scores were used to compare MD between subjects and controls, and among subgroups (Mann-Whitney). False discovery rate (FDR) adjustment was used for multiple comparison correction. For comparison between cortical and subcortical subgroups, a

TABLE 1 Demographics of the healthy controls and sporadic CJD cohort

Group	Number	Sex	Age (years; mean ± SD, median, range)	MMSE (mean ± SD, median, range)	Barthel index score (mean ± SD, median, range)	Time-ratio ^a (mean ± SD, median, range)	Total disease duration (months; mean ± SD, median, range)	Codon 129 (n = 37)	Molecular classification ^b
Type ^c (n = 27; 73%)									
n (%)									
HC	30	15F (50%) 15M (50%)	63.4 ± 10.5 66.5 [45–78]	29.36 ± 1.03 30 [26–30]	N/D	N/A	N/A	N/A	N/A
sCJD	37	17F (46%) 20M (54%)	64 ± 7.8 65 [46–82]	16 ± 8.5 18 [0–27]	63.7 ± 37 70 [0–100]	0.64 ± 0.25 0.71 [0.11–0.99]	16.27 ± 8.19 17 [3–34]	MM (n = 12, 32.4%) MM2C MM1-2C MM N/A MV (n = 18, 48.6%) MV1 MV2C MV2K MV2K+C MV1-2 MV N/A VV (n = 7, 19%) VV1 VV2 VV1-2 VV N/A	1 (2.7%) 7 (18.9%) 2 (5.4%) 2 (5.4%) 4 (10.8%) 4 (10.8%) 2 (5.4%) 1 (2.7%) 2 (5.4%) 4 (10.8%) 1 (2.7%) 3 (8.1%) 1 (2.7%) 2 (5.4%)

Abbreviations: HC, healthy controls; M, methionine; MMSE, Mini-Mental State Examination; n = number of cases; N/A, data not applicable; N/D, not done; V, valine.

^aTime-ratio is defined as ratio of time from disease onset to MRI/total disease duration. In examining the sCJD group subdivisions, the subcortical sCJD group had an average time ratio of 0.47–0.99), whereas the cortical group had an average time ratio of 0.59 (range 0.11–0.91), so the cortical subgroup had their brain MRI for this study slightly earlier in their disease course.

^bCodon 129 data were available in all 37 patients, but prion typing on western blot was available only in the 27 pathology-proven cases and not in the 10 cases not pathology-proven (“probable sCJD;” see text). Percentages might not add exactly due to rounding.

^cAll MM2 cases with a final pathologic diagnosis and molecular classification were cortical type (MM2-C).

TABLE 2 Average grey matter (GM) mean diffusivity (MD) in sporadic Creutzfeldt–Jakob disease cohort by group-wise analysis

	Mean diffusivity (MD)			
	HC		sCJD	
Cortical MD	779 ± 61		745 ± 53 ($p < .0001$)	
Subcortical MD	663 ± 92		607 ± 93 ($p < .0001$)	
Cerebellum MD	665 ± 27		685 ± 36 ($p < .05$)	
GM volumes of interest (VOI)	Mean diffusivity (MD)			
	Left		Right	
	HC	sCJD	HC	sCJD
<i>Frontal</i>				
Caudal middle-frontal	753 ± 26	743 ± 33	760 ± 38	745 ± 44
Lateral orbito-frontal	739 ± 38	729 ± 64	733 ± 25	722 ± 73
Medial orbito-frontal	800 ± 20	783 ± 57	760 ± 28	761 ± 79
Paracentral	814 ± 41	806 ± 61	786 ± 35	759 ± 67
Pars opercularis	773 ± 21	773 ± 50	767 ± 24	749 ± 56
Pars orbitalis	781 ± 24	770 ± 66	787 ± 29	748 ± 92*
Pars triangularis	789 ± 22	781 ± 58	762 ± 38	741 ± 55
Precentral	760 ± 25	746 ± 31	768 ± 30	756 ± 34
Rostral middle-frontal	794 ± 21	765 ± 53*	782 ± 27	751 ± 62*
Superior frontal	802 ± 18	783 ± 36	788 ± 22	772 ± 46
Frontal pole	634 ± 189	546 ± 170	587 ± 178	582 ± 197
<i>Parietal</i>				
Inferior parietal	771 ± 23	711 ± 72*	770 ± 33	699 ± 98*
Postcentral	772 ± 24	757 ± 38	765 ± 29	757 ± 60
Precuneus	801 ± 21	728 ± 86*	783 ± 26	713 ± 106*
Superior parietal	756 ± 27	722 ± 55	762 ± 42	735 ± 61**
Supramarginal	785 ± 20	759 ± 61	787 ± 28	762 ± 71
<i>Limbic</i>				
Caudal anterior cingulate	843 ± 40	814 ± 71	818 ± 35	795 ± 70
Isthmus cingulate	780 ± 33	749 ± 89	752 ± 33	715 ± 113
Posterior cingulate	813 ± 42	752 ± 81*	795 ± 37	730 ± 93**
Rostral anterior cingulate	839 ± 30	835 ± 66	827 ± 35	816 ± 74
Insula	769 ± 24	763 ± 62	769 ± 22	793 ± 54
Amygdala	785 ± 27	762 ± 50	781 ± 22	763 ± 36*
Hippocampus	819 ± 35	819 ± 44	816 ± 33	814 ± 44
<i>Temporal</i>				
Entorhinal	832 ± 36	811 ± 51	803 ± 35	785 ± 53
Fusiform	749 ± 35	717 ± 76	732 ± 39	687 ± 90*
Inferior temporal	701 ± 30	677 ± 71	713 ± 30	665 ± 73*
Middle temporal	768 ± 23	728 ± 73	774 ± 25	710 ± 80**
Temporal pole	852 ± 62	839 ± 95	856 ± 33	835 ± 88
Parahippocampal	759 ± 37	734 ± 70	748 ± 40	717 ± 68
Superior temporal	786 ± 18	768 ± 51	791 ± 16	749 ± 62**
Transverse temporal	821 ± 42	784 ± 58	839 ± 45	829 ± 64
Banks superior temporal sulcus	710 ± 29	691 ± 91	737 ± 34	702 ± 105
<i>Occipital</i>				
Cuneus	855 ± 31	806 ± 77*	834 ± 33	785 ± 99

TABLE 2 (Continued)

GM volumes of interest (VOI)	Mean diffusivity (MD)			
	Left		Right	
	HC	sCJD	HC	sCJD
Lateral occipital	754 ± 22	716 ± 67	743 ± 21	687 ± 80
Lingual	811 ± 28	780 ± 88	814 ± 27	772 ± 95
Pericalcarine	784 ± 40	770 ± 72	775 ± 29	765 ± 81
<i>Subcortical</i>				
Caudate	806 ± 48	776 ± 87*	777 ± 55	728 ± 94*
Putamen	642 ± 41	567 ± 88***	651 ± 41	573 ± 88***
Pallidum	549 ± 43	506 ± 81*	576 ± 43	520 ± 74***
Thalamus	664 ± 24	618 ± 62***	644 ± 23	600 ± 58***
<i>Cerebellum</i>	664 ± 27	683 ± 36*	667 ± 24	687 ± 36*

Note: MD values are reported in $\text{mm}^2/\text{s} \times 10^{-3}$ as average ± standard deviation. HC: Controls. In bold statistically significant average MD reduction in sCJD compared with controls: (***) = $p < .001$, (**) = $p < .005$, and (*) = $p < .05$ (Mann–Whitney test), all FDR corrected. In italics, trend toward reduced average MD with p -values $\geq .05$ and $< .1$. Only for cerebellum, bold italics shows significant increase of average MD in sCJD versus controls; (*) = $p < .05$, FDR corrected. Cortical areas in bold are those considered part of the Default Mode Network (Alves et al., 2019).

MANOVA test (Pillai's trace) was also performed (Pillai, 1955). A $p < .05$ was considered significant. Statistical testing was performed using Real Statistics Resource Pack software (Release 7.6) and JASP Team (2022), JASP (Version 0.16.1).

2.3.2 | Functional imaging

We used SPM12 (Statistical Parametric Mapping, Wellcome Trust Center for Neuroimaging, London, UK) running under Matlab R2014a (MathWorks) to process and analyze functional data. Five initial functional volumes were discarded to allow magnetic field stabilization. Pre-processing of functional images included the following steps: slice time-correction, spatial realignment, coregistration to the subject's structural T1w image, normalization to the MNI T1 space using the SPM segment module, and the default tissue probability map (unified segmentation) (Ashburner & Friston, 2005; Pereira et al., 2013), smoothing with a 6-mm gaussian kernel, and bandpass temporal filtering to preserve frequencies between 0.0083 and 0.15 Hz.

Two spherical seed volume of interest (VOI) with a 5 mm radius were used to derive dorsal and ventral DMN (dDMN and vDMN) (Andrews-Hanna et al., 2010; Damoiseaux, 2012; Jones et al., 2016). The two seeds were located within the right posterior cingulate gyrus (PCC), as one of the main hubs of the DMN (Buckner et al., 2008; Leech & Sharp, 2014), one for each component of the DMN, following the separation of sub-networks as suggested by Jones et al (Jones et al., 2016). The two identified seeds were located at the following MNI coordinates: +16, -48, +34 for the dDMN and +12, -54, +14 for the vDMN, with each seed located within the portion of respectively dDMN and vDMN in the right PCC (based on the singlesubject MD maps as reported in the Supporting Information for further details).

We extracted the average blood oxygen level-dependent signal intensity of all voxels within a given seed for each volume throughout

each participant's scan using the MARSBAR toolbox for SPM12 (Brett et al., 2002). Resulting region of interest time series served as covariates of interest for whole-brain voxelwise regression analyses, resulting in a dDMN and vDMN parameter estimate maps for each participant. Covariates of no interest included the mean deep white matter and CSF time-series, the three rotational and three translational motion parameters, the temporal derivative of each of these terms, and the square of all terms (Satterthwaite et al., 2013).

Dorsal and ventral DMN connectivity were examined at a group level. To correct for motion, we used the sum displacement measure during rs-fMRI acquisition as a covariate. Significance was set at a $p < .05$ FWE corrected, at clusterwise level.

3 | RESULTS

3.1 | Subjects

Description of the subjects and controls are reported in Table 1. The entire sCJD cohort on average had moderate dementia and was mild/moderately functionally impaired, although there was a wide range of impairment. Codon 129 polymorphism distribution in our cohort was over-represented for MV and VV and under-represented for MM (Chi-Square, $p < .001$) (Collins et al., 2006; Parchi et al., 1999). Regarding sCJD molecular classification, the cohort was underrepresented for MM1 and overrepresented for MM2, VV1/2, MV1, and MV1/2 (Kolmogorov–Smirnov, $p = .001$; Table S1A,B) (Collins et al., 2006; Parchi et al., 1999).

The 17 subjects included in the rs-fMRI analysis had the following molecular classifications: 1 MM1, 3 MV1, 2 MM2C, 3 MV2C, 2 MV2K, 2 VV2, 1 MV1-2, 1 MM N/A, 1 MV N/A, and 1 VV N/A. They did not differ significantly in MMSE, Barthel score, or time ratio from subjects with only the diffusion dataset (Mann–Whitney, $p > .05$).

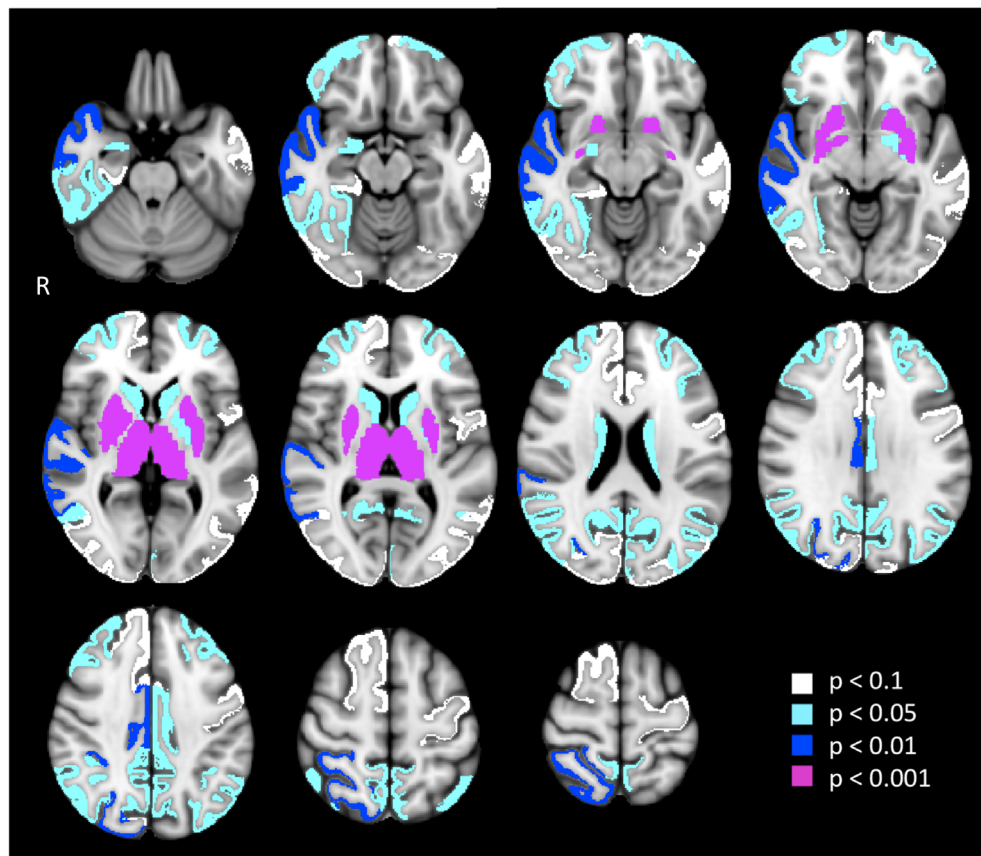


FIGURE 1 Average mean diffusivity (MD) in sporadic Creutzfeldt-Jakob disease (sCJD) subjects versus healthy controls per brain volumes of interest (VOIs), after correction for multiple comparisons (Mann-Whitney, FDR correction). Different p values are reported. The colored areas are regions with significantly reduced (or a trend toward) mean MD in sCJD compared with controls, superposed on the Montreal neurological institute (MNI) atlas. Orientation of image is radiologic (right brain (R) is left side of the image)

3.2 | Grey matter MD analysis

3.2.1 | Regional and VOI analysis of the entire sCJD cohort versus controls

Compared with controls, MD was reduced in sCJD in cortical and in subcortical GM ($p < .0001$), whereas cerebellar MD was increased, compared with controls ($p < .05$) (Table 2, Figure 1). The greatest degree of MD reduction was subcortical, in the thalamus, putamen and GP. Significant MD reduction also was found in the caudate and cortically in two frontal (bilateral rostral-middlefrontal and right pars orbitalis), three parietal (superior and inferior parietal, precuneus), two limbic (PCC and amygdala), four temporal (fusiform, inferior, middle, and superior temporal) and one occipital (cuneus) regions. No supratentorial region showed increased MD compared with controls ($p > .05$).

3.2.2 | Analysis by subgroup: Cortical versus subcortical

In this sub-analysis, we compared each sCJD subgroup (cortical or subcortical) with healthy controls, with a VOI-based analysis. The subcortical subgroup only showed a significant MD reduction for the thalamus, bilaterally ($p < .05$ FDR corrected; Table 3). By contrast, the cortical subgroup showed numerous areas of MD reduction both at

cortical and subcortical level. Specifically, the strongest MD reduction ($p < .001$, FDR corrected) was shown for the left and right inferior parietal cortex, right precuneus, and right middle temporal cortex. Extensive involvement of the parietal cortex was found, bilaterally, in addition to the cuneus and lateral occipital regions, middle and inferior temporal regions, and rostral middle-frontal, among others (Table 3). The cortical subgroup also showed extensive reduction of MD for subcortical regions ($p < .05$, FDR corrected), with the exception of the left thalamus (which showed only a trend toward reduction, $p < .1$) (Table 3). No supratentorial VOI showed a significant increase of MD in sCJD compared with controls. Cerebellar MD was increased in both subgroups compared to HCs, but only the right cerebellar cortex reached a statistical significance ($p < .05$, FDR corrected).

We did not find any statistically significant difference in any supratentorial or cerebellar VOI mean diffusivity when comparing cortical and subcortical subgroups in a VOI-based analysis (Mann-Whitney test, $p > .05$ FDR corrected). Therefore, we performed an additional analysis by clustering cortical regions into five lobar VOIs (frontal, parietal, limbic, temporal, occipital) and combining deep nuclei (caudate, GP, putamen, and thalamus) into a single VOI (VOIs are grouped as in Table 2) to search for any “regional” behavior (data not shown in tables). The subcortical subgroup showed a significant MD reduction in the deep nuclei compared with the cortical sCJD subgroup (MANOVA test, $p = .0107$). By contrast, the cortical sCJD subgroup demonstrated lower parietal ($p = .044$) and limbic GM MD ($p < .001$) compared with the subcortical sCJD subgroup. There was no

TABLE 3 Average grey matter (GM) mean diffusivity (MD) in sporadic Creutzfeldt–Jakob disease pathology-proven cohort by subgroup-wise analysis (cortical and subcortical sCJD subtypes^a)

GM volumes of interest (VOI)	Mean diffusivity (MD)					
	Left			Right		
	HC	Cortical subtype sCJD (n = 19)	Subcortical subtype sCJD (n = 5)	HC	Cortical subtype sCJD (n = 19)	Subcortical subtype sCJD (n = 5)
<i>Frontal</i>						
Caudal middle-frontal	753 ± 26	743 ± 32*	753 ± 29	760 ± 38	745 ± 43*	763 ± 31
Lateral orbito-frontal	739 ± 38	734 ± 81	760 ± 46	733 ± 25	726 ± 79	774 ± 57
Medial orbito-frontal ^b	800 ± 20	783 ± 62	798 ± 44	760 ± 28	761 ± 91	792 ± 70
Paracentral	814 ± 41	746 ± 39	809 ± 92	786 ± 35	759 ± 73	740 ± 67
Pars opercularis	773 ± 21	773 ± 55	791 ± 56	767 ± 24	749 ± 67	763 ± 49
Pars orbitalis	781 ± 24	770 ± 67	815 ± 63	787 ± 29	748 ± 109**	812 ± 61
Pars triangularis	789 ± 22	781 ± 68*	796 ± 61	762 ± 38	741 ± 51	773 ± 50
Precentral	760 ± 25	746 ± 39*	754 ± 13	768 ± 30	756 ± 39	764 ± 27
Rostral middle-frontal	794 ± 21	765 ± 53**	797 ± 19	782 ± 27	751 ± 64**	815 ± 42
Superior frontal	802 ± 18	783 ± 36*	796 ± 37	788 ± 22	772 ± 50*	785 ± 46
Frontal pole	634 ± 189	546 ± 175*	485 ± 132	587 ± 178	592 ± 202	699 ± 170
<i>Parietal</i>						
Inferior parietal	771 ± 23	715 ± 55***	782 ± 27	770 ± 33	699 ± 88***	769 ± 53
Postcentral	772 ± 24	757 ± 41*	772 ± 33	765 ± 29	757 ± 70	776 ± 56
Precuneus	801 ± 21	739 ± 89**	788 ± 59	783 ± 26	713 ± 111***	778 ± 63
Superior parietal	756 ± 27	722 ± 66**	749 ± 36	762 ± 42	735 ± 57**	786 ± 22
Supramarginal	785 ± 20	759 ± 63**	808 ± 27	787 ± 28	762 ± 83**	804 ± 42
<i>Limbic</i>						
Caudal anterior cingulate	843 ± 40	814 ± 71	844 ± 83	818 ± 35	795 ± 81	791 ± 86
Isthmus cingulate	780 ± 33	749 ± 87	779 ± 62	752 ± 33	715 ± 119	796 ± 51
Posterior cingulate	813 ± 42	757 ± 98**	797 ± 62	795 ± 37	730 ± 106**	756 ± 74
Rostral anterior cingulate	839 ± 30	846 ± 81	873 ± 83	827 ± 35	816 ± 89	851 ± 53
Insula	763 ± 69	762 ± 56	844 ± 83	769 ± 22	793 ± 57	827 ± 65
Amygdala	785 ± 27	762 ± 41	767 ± 93	781 ± 22	763 ± 27*	764 ± 43
Hippocampus	819 ± 35	819 ± 46	815 ± 23	816 ± 33	821 ± 45	816 ± 41
<i>Temporal</i>						
Entorhinal	832 ± 36	811 ± 55	789 ± 59	803 ± 35	785 ± 59	767 ± 72
Fusiform	749 ± 35	717 ± 86*	761 ± 39	732 ± 39	687 ± 106*	723 ± 60
Inferior temporal	701 ± 30	677 ± 78*	728 ± 51	713 ± 30	665 ± 79**	697 ± 70
Middle temporal	768 ± 23	729 ± 71**	792 ± 35	774 ± 25	710 ± 83***	767 ± 52
Temporal pole	852 ± 62	839 ± 95	803 ± 234	856 ± 33	835 ± 110	895 ± 54
Parahippocampal	759 ± 37	734 ± 87	744 ± 29	748 ± 40	717 ± 74	811 ± 55
Superior temporal	786 ± 18	768 ± 56*	800 ± 46	791 ± 16	749 ± 62**	738 ± 70
Transverse temporal	821 ± 42	784 ± 59*	836 ± 38	839 ± 45	829 ± 74	860 ± 56
Banks sup. Temp. Sulcus	710 ± 29	691 ± 102*	744 ± 84	737 ± 34	702 ± 116	755 ± 101
<i>Occipital</i>						
Cuneus	855 ± 31	806 ± 78**	858 ± 28	834 ± 33	785 ± 119**	842 ± 20
Lateral occipital	754 ± 22	716 ± 65**	759 ± 38	743 ± 21	687 ± 82**	733 ± 38
Lingual	811 ± 28	780 ± 98	831 ± 42	814 ± 27	772 ± 108	822 ± 35
Pericalcarine	784 ± 40	774 ± 80	807 ± 56	775 ± 29	765 ± 95	799 ± 36

(Continues)

TABLE 3 (Continued)

GM volumes of interest (VOI)	Mean diffusivity (MD)					
	Left			Right		
	HC	Cortical subtype sCJD (n = 19)	Subcortical subtype sCJD (n = 5)	HC	Cortical subtype sCJD (n = 19)	Subcortical subtype sCJD (n = 5)
<i>Subcortical</i>						
Caudate	806 ± 48	776 ± 79*	767 ± 93	777 ± 55	728 ± 94*	725 ± 79
Putamen	642 ± 41	567 ± 86*	589 ± 75	651 ± 41	573 ± 85*	595 ± 74
Pallidum	549 ± 43	506 ± 92*	537 ± 35	576 ± 43	520 ± 86*	520 ± 55
Thalamus	664 ± 24	618 ± 56	579 ± 37*	644 ± 23	600 ± 61*	569 ± 24*
<i>Cerebellum</i>	664 ± 27	683 ± 38	708 ± 32	667 ± 24	687 ± 31*	709 ± 32

Note: MD values are reported in $\text{mm}^2/\text{s} \times 10^{-3}$ as average \pm standard deviation. HC: Controls. In bold statistically significant average MD difference (positive or negative) between sCJD and controls: (***) = $p < .001$, (**) = $p < .005$, and (*) = $p < .05$ (Mann Whitney test), all FDR corrected. In italics, trend toward reduced average MD with p -values $\geq .05$ and $< .1$. Only for cerebellum, bold italics shows significant increase of average MD in sCJD versus controls; (*) = $p < 0.05$, FDR corrected. Cortical subregions in bold are those considered part of the Default Mode Network (Alves et al., 2019).

^aThe pathology-proven sCJD subjects were divided in two different subgroups based on molecular classification: a cortical-predominant subtype, "cortical subtype," including MM(V)1, MM(V)2C, and VV1 subtypes and a subcortical-predominant subtype, "subcortical subtype" including VV2 and MV2K subtypes (see text).

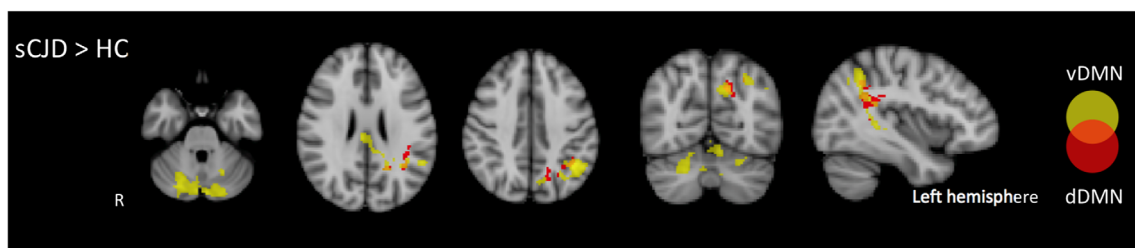


FIGURE 2 Intrinsic resting-state connectivity for ventral DMN (vDMN) and dorsal (dDMN) seeds. Clusters with a family-wise error rate (FWE) corrected p value $< .05$ are reported. Increased connectivity in sCJD subjects compared with healthy controls is shown. Ventral DMN is shown in yellow, dorsal DMN in red; overlap areas are shown in orange. HC, healthy controls. Orientation of image is radiologic (right brain (R) is left side of the image)

statistically significant difference in MD between subgroups in any other supratentorial lobe ($p > .05$).

3.3 | Resting-state functional connectivity

Compared with controls, the sCJD cohort showed no region of decreased vDMN or dDMN connectivity. Rather, increased connectivity was found in sCJD for dDMN and vDMN seeds, with vDMN having more areas with increased connectivity (supramarginal, posterior cingulate, bilateral cerebellar GM) than the dDMN (precuneus) ($p < .05$, FWE corrected). (Figure 2, Table 4).

We did not have sufficient sample sizes to investigate functional differences between sCJD molecular subtypes.

4 | DISCUSSION

Our diffusion imaging study showed relatively predominant involvement of the posterior portion of the DMN together with subcortical grey

matter (striatum, pallidum, and thalamus) in sCJD. For the first time, we identified abnormally increased functional connectivity at rest in sCJD, both in the dorsal and ventral components of the DMN. Our multimodal analysis corroborates our atrophy-based hypothesis that DMN areas are particularly vulnerable in sCJD (Younes et al., 2021).

4.1 | Grey matter mean diffusivity quantification in sCJD

4.1.1 | Subcortical MD

We showed significant MD reduction in our sCJD cohort in the caudate and putamen, consistent with traditional visual assessment studies of conventional three-directions DWI/ADC images (Meissner et al., 2009; Shiga et al., 2004; Vitali et al., 2011) and also with our previous MD quantification study at 1.5T (Caverzasi, Henry, et al., 2014). We also confirmed our prior finding that despite DWI/ADC abnormalities being less common in the thalamus (than striatum or cortex) and very rare in the GP by visual assessment (Meissner et al., 2009; Murata et al., 2002; Vitali

TABLE 4 Resting state DMN connectivity of sCJD subjects versus controls

Contrast	Region containing peak voxel	BA	MNI x, y, z coordinates	Peak T	Size
(a) for ventral DMN (vDMN) seed					
sCJD > HC	Cerebellum crus I R	-	24, -78, -26	6.13	1198
	Cerebellum crus II L	-	-2, -82, -30	5.97	
	Cerebellum crus II L	-	-18, -84, -32	5.48	
	Supramarginal L	40	-42, -54, 40	6.00	1204
	Precuneus L	7	-14, -64, 34	5.94	
	Superior temporal L	41	-32, -44, 18	4.92	
	Posterior cingulate R	23	4, -26, 26	4.99	196
(b) for dorsal DMN (dDMN) seed					
sCJD > HC	Precuneus L	18	-24, -44, 8	4.76	399
	Superior temporal L	39	-32, -42, 30	4.07	
	Angular L	40	-36, -52, 26	4.06	
	Precuneus L	18	-16, -66, 38	4.82	129

Note: Task-free fMRI analysis clusters with a family-wise error rate (FWE) corrected *p* value < .05. Coordinates are reported in Montreal Neurological Institute (MNI) template space. *T*-score for each cluster is reported as Peak T. Size is reported in voxels (voxel size = 2.0 × 2.0 × 2.0 mm³). Reported supratentorial regions follow cortical and subcortical parcellation by Desikan et al. (2006) and Fischl et al. (2002), infratentorial parcellation follows that of Schmahmann et al. (1999). Significant clusters are shown in bold font with their significant subclusters (from different but nearby anatomic regions) shown indented in regular font. Abbreviations: BA, brodmann area; HC, healthy controls; L, left; R, right.

et al., 2011), these regions showed significant MD reduction at 3T (Figure 1, Table 2), with even greater significance than in our prior 1.5T study (Caverzasi, Henry, et al., 2014). In fact, the thalami showed the most significant MD reduction across all subcortical VOIs (Table 2). This was surprising as the most sCJD patients do not have thalamic involvement by visual assessment, and even in molecular subtypes with common thalamic FLAIR/DWI involvement, less than 50% of cases have abnormal thalami by visual assessment (Meissner et al., 2009). Grau-Rivera and colleagues with a ROI-based analysis found significant deep nuclei MD reduction, also with a few thalamic nuclei with increased MD, in a cohort of 13 sCJD and two E200K genetic prion cases (Grau-Rivera et al., 2017). Given its high degree of interconnection, the thalamus has been proposed as a relay center of primary importance in prion diseases (Grau-Rivera et al., 2017). Clinical and experimental evidence has suggested early thalamic involvement in prion disease (Jeffrey et al., 2000; Lee et al., 2009; Tschampa et al., 2002); typical sCJD symptoms as myoclonus and periodic sharp wave complexes have been associated with thalamic involvement in the disease (Tschampa et al., 2002). The lack of clear signal abnormality by visual assessment in the GP has been attributed to possible interference from iron deposition (Lin et al., 2006), but this does not explain why the thalamus is not as frequently involved by visual assessment (Lin et al., 2006; Meissner et al., 2009; Tschampa et al., 2003; Vitali et al., 2011).

4.1.2 | Cortical MD

In the cortex, we found the most significant MD reduction in posterior cingulate, superior parietal, middle and inferior temporal regions,

which are known to be part of DMN, also consistent with our prior study at 1.5T (Caverzasi, Henry, et al., 2014) (Table 2, Figure 1). The only other study examining MD at 3T in sCJD did not find any significant cortical MD reduction, but found increased MD in subcortical white matter and a few subcortical regions (Grau-Rivera et al., 2017). One possible reason for the different findings is that Grau-Rivera et al. included E200K genetic in their cohort, which generally has more predominant subcortical than cortical involvement (Lee et al., 2010). Furthermore, Grau-Rivera et al. did not have an analysis with all CJD subtypes combined (as we have)—they divided them into CJD and fatal insomnia (FI) based on clinical characterization. No insular or precentral cortex involvement was demonstrated by our 3T quantitative analysis, as per our previous 1.5T analysis (Caverzasi, Henry, et al., 2014). The lack of insular involvement in the present study is also consistent with the choice of excluding insula in proposed MRI diagnostic criteria (Bizzi et al., 2020; Vitali et al., 2011).

4.2 | Analysis by cortical and subcortical sCJD subgroups

4.2.1 | Subcortical MD

We demonstrated that, compared with controls, the subcortical sCJD subgroup (i.e., MV2K and VV2, *n* = 5) had reduced MD in all subcortical VOIs, yet only thalami reached statistical significance (after correction for FDR), whereas the cortical sCJD subgroup had a significant MD reduction in all subcortical VOIs (with the exception of left thalamus). The paucity of findings in the subcortical sCJD subgroup is most

likely due to the very small number of cases available for this analysis ($n = 5$). The extensive and bilateral MD reduction within subcortical GM regions of the cortical sCJD subgroup and the limited involvement (only the thalamus) in the subcortical sCJD subgroup is only partially surprising. Indeed, these findings fit into the model of disease propagation proposed in literature (Caverzasi, Henry, et al., 2014; Pascuzzo et al., 2020), once we consider that sCJD subjects enrolled in the current study had on average a relatively advanced stage of illness (time ratio = 0.64 ± 0.25 , median = 0.71). At this stage of disease, subcortical regions of the subcortical sCJD subgroup (characterized by early subcortical involvement) may have already pseudo-normalized their mean diffusivity signal (Caverzasi, Henry, et al., 2014) and, by contrast, they may have been more recently affected by the disease in the cortical sCJD subgroup (e.g., with more pronounced MD reduction).

4.2.2 | Cortical MD

As expected, the sCJD cortical subgroup had multiple cortical regions with significant MD reduction, including the entire parietal lobe (surprisingly including the left postcentral, which is usually spared by visual assessment of DWI/ADC), cuneus, lateral occipital regions, and parts of the temporal (middle and inferior temporal above all) and frontal lobes (Table 2). This pattern of involvement greatly overlaps with the DMN (Alves et al., 2019), except for sparing of involvement in our cohort of the medial orbito-frontal regions. This pattern of cortical involvement is consistent with what was found by Pascuzzo and colleagues using a visual assessment approach (Pascuzzo et al., 2020). The subcortical sCJD group, instead, showed no area of cortical MD reduction despite being slightly more advanced in the disease time course compared with the cortical subgroup (subcortical group average time ratio = 0.73, range = 0.47–1; cortical group average time ratio = 0.59, range 0.11–0.91). This may indicate greater variability than expected in the spreading of diffusion abnormalities from subcortical toward cortical regions in this sCJD subgroup. One must take into consideration, however, that this finding is based on a limited number of subjects ($n = 5$).

When we explored differences between subgroups, we found that the cortical sCJD subgroup had a significantly lower MD in the parietal and limbic lobes compared with the subcortical subgroup. The more extensive involvement of the parietal cortex in the cortical subgroup was expected based on the propagation model by Pascuzzo and colleagues mentioned above. That we found greater limbic involvement (hippocampus, amygdala, and cingulate) in the cortical than the subcortical subgroup was surprising, because Pascuzzo et al. found in intermediate to late-intermediate stages of the disease propagation model that these regions seemed to be affected in both subgroups (Pascuzzo et al., 2020). Further diffusivity studies based on larger datasets are needed to better investigate these overlapping yet distinct findings between the two studies.

4.3 | Increased cerebellar mean diffusivity in sCJD

In contrast to most supratentorial regions, the cerebellar cortex of the sCJD cohort had increased MD compared with controls (Table 2). This finding corroborates the sparse literature on cerebellar GM diffusivity in prion diseases, which showed increased ADC (assessed by conventional three-directions DWI) (Cohen et al., 2009) or increased MD (with a DTI approach)(Grau-Rivera et al., 2017). Such a different pattern of diffusion changes between cerebellar and supratentorial regions has been previously explained as possibly due to different underlying pathological substrates (Cohen et al., 2009) or time sequence of pathology (Iwasaki, 2017; Parchi et al., 1999, 2011), slightly different forms of prions affecting the cerebellum (Puoti et al., 1999), and/or different neurochemical changes than elsewhere (Ferrer et al., 2000). At our subgroup-level analysis, only the cortical sCJD subgroup showed a significant MD increase compared with controls (and only for the right cerebellar cortex). This finding of increased cerebellar MD can be explained by the quasi-J-shaped curve of MD changes over time in sCJD (Caverzasi, Henry, et al., 2014) and Pascuzzo and colleagues' model (Pascuzzo et al., 2020). Indeed, based on the model by Pascuzzo et al., the subcortical sCJD subgroup presents with early involvement of the cerebellum, whereas the cortical subgroup shows later cerebellar involvement. The model by Pascuzzo et al. also fits with what is known clinically in sCJD, that the subcortical group subtypes (VV2 and MV2) usually present with early cerebellar features, such as ataxia (Parchi et al., 1999). Although only our cortical subgroup had statistically significant increased MD, and only in the right cerebellum, even the left cerebellum was higher than controls (although not statistically significant), and the subcortical group cerebellum showed the highest MD (also not statistically significant, likely due to the small sample size).

4.4 | Increased DMN connectivity in sCJD

In our resting-state fMRI analysis, we found an increased connectivity in sCJD both for dDMN and vDMN seeds, with more areas involved for the vDMN (Figure 2, Table 4). A topographic division of DMN into ventral (vDMN) and dorsal (dDMN) components has been proposed in the literature (Andrews-Hanna et al., 2010; Damoiseaux, 2012; Jones et al., 2016), with the vDMN being linked to internally directed thought at rest, including memory retrieval and planning, and the dDMN being involved with the control of attentional focus and having a high degree of interconnections with other cognitive networks (Fornito et al., 2012; Leech et al., 2012; Leech & Sharp, 2014; Margulies et al., 2009). As both DMN components support dissociable cognitive processes, it is possible that the lesser involvement of the dDMN in sCJD in this study is related to the relatively less involvement of mesial frontal regions in our cohort compared with involvement of other DMN regions in our sCJD cohort (Table 2). Regarding the cerebellum, as with some bilateral cortical regions, it showed increased vDMN connectivity (Figure 2, Table 4) (Buckner et al., 2011; Yeo et al., 2011). Examining our diffusion and functional

data, the cerebellar response to prion involvement may differ from that of supratentorial cortical and subcortical regions. Despite the cerebellum having increased MD and cortex having reduced MD, in fact, both show increased functional connectivity.

Increased connectivity of resting-state functional networks has been described in a spectrum of neuropsychiatric and neurodegenerative diseases, including amyotrophic lateral sclerosis (Zhou et al., 2013), subjects at risk of Alzheimer's disease (Filippini et al., 2009; Hafkemeijer et al., 2013; Kerestes et al., 2015; Petrella et al., 2011), and schizophrenia (Whitfield-Gabrieli et al., 2009), especially in the prodromal state. Different explanations have been proposed including compensatory mechanisms occurring with relatively low disease burden (Agosta et al., 2013; Farb et al., 2013; Zhou et al., 2013) in an attempt to recruit relatively preserved areas in order to maintain function, a maladaptive response of hyperconnectivity to an underlying pathologic process, and/or to excitatory-inhibitory imbalance of functional networks (Douaud et al., 2011; Farb et al., 2013; Lehmann et al., 2015; Pievani et al., 2014; Wu et al., 2009; Zhou et al., 2010). The functional connectivity abnormality in sCJD raises questions regarding how neurodegenerative diseases spread in the brain, and whether there are common pathways of spreading, despite diverse pathologic entities (Brettschneider et al., 2015; Frost & Diamond, 2009; Raj et al., 2012; Sanders et al., 2016; Seeley et al., 2009; Stopschinski & Diamond, 2017; Watts & Prusiner, 2014). Misfolded proteins in neurodegenerative disease show propagation along neural processes, involving local and subsequently long-range circuits via trans-synaptic spread (Holmes & Diamond, 2012; Scott et al., 1992). Disease spreading might be predicted according to a number of structural, metabolic, physiologic, and functional networks (Raj et al., 2012; Zhou et al., 2012). Improved understanding of functional connectivity in neurodegenerative diseases could stimulate development of new network-based diagnostics and allow improved monitoring of disease progression for treatment trials. This might be even more true for rapidly progressive dementias, such as prion diseases, in which there is a great need for better outcomes than survival (Mead et al., 2011).

4.5 | Study limitations

Several limitations apply to our study, some of which have already been discussed. Although our cohort included only 37 subjects, it was very large for a quantitative imaging study in prion disease and has the advantage of the homogeneity of images obtained at a single site. As already mentioned, our cohort was overrepresented by some slower progressing subtypes, with fewer faster progressing molecular subtypes (e.g., MM1 and VV2) and had a different proportion of the three Codon 129 subtypes than present in large multinational cohorts. Although all molecular subtypes were represented in our final study cohort, patients with too much motion artifact (which likely was more common in faster progressing sCJD subtypes) for volumetric T1 and/or HARDI analyses were not included. Thus, our results might be more relevant to the slower progressing group of patients or those in

less advanced stages of disease regardless of molecular subtype. Our patients were on average mild to moderately functionally impaired based on Barthel median score of 70/100 and they were about 2/3 of the way through their disease course.

Partial volume effects of CSF adjacent to grey matter would result in increased MD in the adjacent grey matter regions. Thus, if we had accounted for partial volume effects in this study, this would have led to removing this increased MD effect, resulting in making it more likely to find reduced MD. We therefore conservatively decided to not account for partial volume effects in our diffusion analysis, reducing the likelihood of finding reduced MD. Thus, there is probably even greater reduced MD in the caudate, cortex, and possibly thalamic regions than we have reported here.

Regarding our rs-fMRI dataset, motion could have affected our results, as clinically advanced subjects are more prone to motion during MRI acquisition. We excluded, however, only two subjects out of 19 and motion was used as an additional covariate for network analysis. Thus, we do not think motion artifact affected our results significantly. Larger sample sizes, however, would allow us to confirm our results and better detect abnormal connectivity in each sCJD molecular subtype.

Lastly, although we acquired serial imaging on most subjects, because of the difficulty in acquiring serial imaging of sufficient quality due to the rapidity of disease progression, we were unable to perform longitudinal analyses.

5 | CONCLUSIONS

Our quantitative analysis of GM diffusivity in sCJD at 3T confirmed our prior findings at 1.5T of predominant MD reduction in subcortical, retrosplenial, parietal-occipital, and temporal regions (Caverzasi, Henry, et al., 2014), largely part of the Default Mode Network, and we also confirmed increased MD in the cerebellum previously reported by others (Grau-Rivera et al., 2017). We also found, quantitatively, MD reduction in cortical and subcortical subgroups of sCJD based on molecular classification. Assessing resting-state functional connectivity in prion disease for the first time, we identified increased connectivity of the Default Mode Network in sCJD, in parallel to extensive parietal and temporal reduced mean diffusivity. In prion disease, rs-fMRI might represent a useful additional tool to understand underlying disease physiology and perhaps even predict progression, providing new tools to track of disease involvement and progression.

AUTHOR CONTRIBUTIONS

Matteo Paoletti, Eduardo Caverzasi, and Michael D. Geschwind have made substantial contribution to conception and design of the study. Maria Luisa Mandelli and Jesse A. Brown contributed in the analysis and interpretation of data. All authors have been involved in drafting the manuscript and in revising it critically for important intellectual content. All authors approved the final version of the manuscript draft. All authors agree to be accountable for all aspects of the presented work.

ACKNOWLEDGMENTS

The authors want to thank patients and their families for their generous participation to this study. A special thank goes to Prof. Brian S. Appleby and to Prof. Mark Cohen, Case Western Reserve University, OH, for their help in reviewing the autopsy data. They also want to thank Dr. Elena Ballante (Biodata Center, Mondino Foundation, Pavia, Italy) for her help with statistical analysis.

CONFLICT OF INTEREST

MP, EC, MLM, JB, RH, BM, HR, and SB have no conflict of interest related to this paper. MDG has consulted for Bioscience Pharma Partners LLC and Clearview Healthcare Partners and done medical legal consulting related to prion disease; he also consults or has consulted for Quest Diagnostics Inc., Biohaven Pharmaceuticals, Teva Pharmaceuticals, Gerson-Lehrman Group, InSight Consulting, Grand Rounds, Best Doctors, Advanced Medical, Guidepoint Global, and done other medical-legal consulting.

ENROLLMENT INCLUSION AND EXCLUSION CRITERIA

Subjects enrolled for this study are inclusive of all persons without limitations by (1) sex or gender, (2) race or ethnicity, or (3) age other than as scientifically justified.

DATA AVAILABILITY STATEMENT

The data that support the findings of this study are available from the corresponding author upon reasonable request.

ORCID

Matteo Paoletti  <https://orcid.org/0000-0002-1221-7747>

Eduardo Caverzasi  <https://orcid.org/0000-0002-0350-0460>

Maria Luisa Mandelli  <https://orcid.org/0000-0002-2518-2520>

Jesse A. Brown  <https://orcid.org/0000-0002-3139-9451>

Roland G. Henry  <https://orcid.org/0000-0002-8232-7562>

Bruce L. Miller  <https://orcid.org/0000-0002-2152-4220>

Howard J. Rosen  <https://orcid.org/0000-0001-9281-7402>

William W. Seeley  <https://orcid.org/0000-0003-1410-2027>

Michael D. Geschwind  <https://orcid.org/0000-0003-2861-3776>

REFERENCES

- Agosta, F., Canu, E., Valsasina, P., Riva, N., Prella, A., Comi, G., & Filippi, M. (2013). Divergent brain network connectivity in amyotrophic lateral sclerosis. *Neurobiology of Aging, 34*(2), 419–427.
- Alves, P. N., Foulon, C., Karolis, V., Bzdok, D., Margulies, D. S., Volle, E., & Thiebaut de Schotten, M. (2019). An improved neuroanatomical model of the default-mode network reconciles previous neuroimaging and neuropathological findings. *Communications Biology, 2*, 370.
- Andrews-Hanna, J. R., Reidler, J. S., Sepulcre, J., Poulin, R., & Buckner, R. L. (2010). Functional-anatomic fractionation of the brain's default network. *Neuron, 65*(4), 550–562.
- Ashburner, J., & Friston, K. J. (2005). Unified segmentation. *Neuroimage, 26*, 839–851.
- Bizzi, A., Pascuzzo, R., Blevins, J., Grisoli, M., Lodi, R., Moscatelli, M. E. M., Castelli, G., Cohen, M. L., Schonberger, L. B., Foutz, A., Safar, J. G., Appleby, B. S., & Gambetti, P. (2020). Evaluation of a new criterion for detecting prion disease with diffusion magnetic resonance imaging. *JAMA Neurology, 77*(9), 1141–1149.
- Bizzi, A., Pascuzzo, R., Blevins, J., Moscatelli, M. E. M., Grisoli, M., Lodi, R., Doniselli, F. M., Castelli, G., Cohen, M. L., Stamm, A., Schonberger, L. B., Appleby, B. S., & Gambetti, P. (2021). Subtype diagnosis of sporadic Creutzfeldt–Jakob disease with diffusion magnetic resonance imaging. *Annals of Neurology, 89*(3), 560–572.
- Brett, M., Anton, J.-L.L., Valabregue, R., & Poline, J.-B. (2002). Region of interest analysis using an SPM toolbox—Abstract Presented at the 8th International Conference on Functional Mapping of the Human Brain, June February 6, 2002, Sendai, Japan. *Neuroimage, 13*(2), 210–217.
- Brettschneider, J., Del Tredici, K., Lee, V. M.-Y., & Trojanowski, J. Q. (2015). Spreading of pathology in neurodegenerative diseases: A focus on human studies. *Nature Reviews Neuroscience, 16*(2), 109–120.
- Brown, P., Cathala, F., Castaigne, P., & Gajdusek, D. C. (1986). Creutzfeldt–Jakob disease: Clinical analysis of a consecutive series of 230 neuropathologically verified cases. *Annals of Neurology, 20*(5), 597–602.
- Buckner, R. L., Andrews-Hanna, J. R., & Schacter, D. L. (2008). The brain's default network. *Annals of the New York Academy of Sciences, 1124*(1), 1–38.
- Buckner, R. L., Krienen, F. M., Castellanos, A., Diaz, J. C., & Yeo, B. T. T. (2011). The organization of the human cerebellum estimated by intrinsic functional connectivity. *Journal of Neurophysiology, 106*, 2322–2345.
- Caverzasi, E., Henry, R. G., Vitali, P., Lobach, I. V., Kornak, J., Bastianello, S., Dearmond, S. J., Miller, B. L., Rosen, H. J., Mandelli, M. L., & Geschwind, M. D. (2014). Application of quantitative DTI metrics in sporadic CJD. *Neuroimage: Clinical, 4*, 426–435.
- Caverzasi, E., Mandelli, M. L., DeArmond, S. J., Hess, C. P., Vitali, P., Papinutto, N., Oehler, A., Miller, B. L., Lobach, I. V., Bastianello, S., Geschwind, M. D., & Henry, R. G. (2014). White matter involvement in sporadic Creutzfeldt–Jakob disease. *Brain, 137*(Pt 12), 3339–3354.
- Cohen, O. S., Hoffmann, C., Lee, H., Chapman, J., Fulbright, R. K., & Prohovnik, I. (2009). MRI detection of the cerebellar syndrome in Creutzfeldt–Jakob disease. *Cerebellum, 8*(3), 373–381.
- Collins, S. J., Sanchez-Juan, P., Masters, C. L., Klug, G. M., Van Duijn, C., Poleggi, A., Pocchiari, M., Almonti, S., Cuadrado-Corralles, N., De Pedro-Cuesta, J., Budka, H., Gelpi, E., Glatzel, M., Tolnay, M., Hewer, E., Zerr, I., Heinemann, U., Kretschmar, H. a., Jansen, G. H., ... Will, R. G. (2006). Determinants of diagnostic investigation sensitivities across the clinical spectrum of sporadic Creutzfeldt–Jakob disease. *Brain, 129*(9), 2278–2287.
- Damoiseaux, J. S. (2012). Resting-state fMRI as a biomarker for Alzheimer's disease? *Alzheimer's Research & Therapy, 4*(2), 8.
- Desikan, R. S., Ségonne, F., Fischl, B., Quinn, B. T., Dickerson, B. C., Blacker, D., Buckner, R. L., Dale, A. M., Maguire, R. P., Hyman, B. T., Albert, M. S., & Killiany, R. J. (2006). An automated labeling system for subdividing the human cerebral cortex on MRI scans into gyral based regions of interest. *Neuroimage, 31*(3), 968–980.
- Dopper, E. G. P., Rombouts, S. A. R. B., Jiskoot, L. C., Den Heijer, T., De Graaf, J. R. A., De Koning, I., Hammerschlag, A. R., Seelaar, H., Seeley, W. W., Veer, I. M., Van Buchem, M. A., Rizzu, P., & Van Swieten, J. C. (2013). Structural and functional brain connectivity in presymptomatic familial frontotemporal dementia. *Neurology, 80*(9), 814–823.
- Douaud, G., Filippini, N., Knight, S., Talbot, K., & Turner, M. R. (2011). Integration of structural and functional magnetic resonance imaging in amyotrophic lateral sclerosis. *Brain, 134*(12), 3470–3479.
- Eisenmenger, L., Porter, M.-C., Carswell, C. J., Thompson, A., Mead, S., Rudge, P., Collinge, J., Brandner, S., Jäger, H. R., & Hyare, H. (2015). Evolution of diffusion-weighted magnetic resonance imaging signal abnormality in sporadic Creutzfeldt–Jakob disease, with histopathological correlation. *JAMA Neurology, 73*(1), 1.
- Farb, N. A. S., Grady, C. L., Strother, S., Tang-Wai, D. F., Masellis, M., Black, S., Freedman, M., Pollock, B. G., Campbell, K. L., Hasher, L., & Chow, T. W. (2013). Abnormal network connectivity in frontotemporal dementia: Evidence for prefrontal isolation. *Cortex, 49*(7), 1856–1873.

- Ferrer, I., Puig, B., Blanco, R., & Martí, E. (2000). Prion protein deposition and abnormal synaptic protein expression in the cerebellum in Creutzfeldt-Jakob disease. *Neuroscience*, 97(4), 715–726.
- Figini, M., Alexander, D. C., Redaelli, V., Fasano, F., Grisoli, M., Baselli, G., Gambetti, P., Tagliavini, F., & Bizzi, A. (2015). Mathematical models for the diffusion magnetic resonance signal abnormality in patients with prion diseases. *Neuroimage: Clinical*, 7, 142–154.
- Filippini, N., MacIntosh, B. J., Hough, M. G., Goodwin, G. M., Frisoni, G. B., Smith, S. M., Matthews, P. M., Beckmann, C. F., & Mackay, C. E. (2009). Distinct patterns of brain activity in young carriers of the APOE-ε4 allele. *Proceedings of the National Academy of Sciences of the United States of America*, 106(17), 7209–7214.
- Fischl, B., Salat, D. H., Busa, E., Albert, M., Dieterich, M., Haselgrove, C., Van Der Kouwe, A., Killiany, R., Kennedy, D., Klaveness, S., Montillo, A., Makris, N., Rosen, B., & Dale, A. M. (2002). Whole brain segmentation: Automated labeling of neuroanatomical structures in the human brain. *Neuron*, 33, 341–355.
- Fornito, A., Harrison, B. J., Zalesky, A., & Simons, J. S. (2012). Competitive and cooperative dynamics of large-scale brain functional networks supporting recollection. *Proceedings of the National Academy of Sciences of the United States of America*, 109(31), 12788–12793.
- Frost, B., & Diamond, M. I. (2009). Prion-like mechanisms in neurodegenerative diseases. *Nature Reviews Neuroscience*, 11(3), 155–159.
- Gardner, R. C., Boxer, A. L., Trujillo, A., Mirsky, J. B., Guo, C. C., Gennatas, E. D., Heuer, H. W., Fine, E., Zhou, J., Kramer, J. H., Miller, B. L., & Seeley, W. W. (2013). Intrinsic connectivity network disruption in progressive supranuclear palsy. *Annals of Neurology*, 73(5), 603–616.
- Geschwind, M. D. (2015). Prion diseases. *CONTINUUM Lifelong Learning in Neurology*, 21(6), 1612–1638.
- Geschwind, M. D., Josephs, K. A., Parisi, J. E., & Keegan, B. M. (2007). A 54-year-old man with slowness of movement and confusion. *Neurology*, 69(19), 1881–1887.
- Geschwind, M. D., Potter, C. A., Sattavat, M., Garcia, P. A., Rosen, H. J., Miller, B. L., & De Armond, S. J. (2009). Correlating DWI MRI with pathologic and other features of Jakob-Creutzfeldt disease. *Alzheimer Disease and Associated Disorders*, 23, 82–87.
- Grau-Rivera, O., Calvo, A., Bargalló, N., Monté, G. C., Nos, C., Lladó, A., Molinuevo, J. L., Gelpi, E., & Sánchez-Valle, R. (2017). Quantitative magnetic resonance abnormalities in Creutzfeldt-Jakob disease and fatal insomnia. *Journal of Alzheimer's Disease*, 55(1), 431–443.
- Greve, D. N., & Fischl, B. (2009). Accurate and robust brain image alignment using boundary-based registration. *Neuroimage*, 48(1), 63–72.
- Hacker, C. D., Perlmutter, J. S., Criswell, S. R., Ances, B. M., & Snyder, A. Z. (2012). Resting state functional connectivity of the striatum in Parkinson's disease. *Brain*, 135(12), 3699–3711.
- Hafkemeijer, A., Altmann-Schneider, I., Oleksik, A. M., van de Wiel, L., Middelkoop, H. A. M., van Buchem, M. A., van der Grond, J., & Rombouts, S. A. R. B. (2013). Increased functional connectivity and brain atrophy in elderly with subjective memory complaints. *Brain Connectivity*, 3(4), 353–362.
- Hermann, P., Appleby, B., Brandel, J. P., Caughey, B., Collins, S., Geschwind, M. D., Green, A., Haik, S., Kovacs, G. G., Ladogana, A., Llorens, F., Mead, S., Nishida, N., Pal, S., Parchi, P., Pocchiari, M., Satoh, K., Zanusso, G., & Zerr, I. (2021). Biomarkers and diagnostic guidelines for sporadic Creutzfeldt-Jakob disease. *The Lancet Neurology*, 20(3), 235–246.
- Holmes, B. B., & Diamond, M. I. (2012). Cellular mechanisms of protein aggregate propagation. *Current Opinion in Neurology*, 25(6), 1–726.
- Iwasaki, Y. (2017). Creutzfeldt-Jakob disease. *Neuropathology*, 37(2), 174–188.
- Jeffrey, M., Halliday, W. G., Bell, J., Johnston, A. R., Macleod, N. K., Ingham, C., Sayers, A. R., Brown, D. A., & Fraser, J. R. (2000). Synapse loss associated with abnormal PrP precedes neuronal degeneration in the scrapie-infected murine hippocampus. *Neuropathology and Applied Neurobiology*, 26, 41–54.
- Jones, D. T., Knopman, D. S., Gunter, J. L., Graff-Radford, J., Vemuri, P., Boeve, B. F., Petersen, R. C., Weiner, M. W., & Jack, C. R. (2016). Cascading network failure across the Alzheimer's disease spectrum. *Brain*, 139(2), 547–562.
- Kallenberg, K., Schulz-Schaeffer, W. J., Jastrow, U., Poser, S., Meissner, B., Tschampa, H. J., Zerr, I., & Knauth, M. (2006). Creutzfeldt-Jakob disease: Comparative analysis of MR imaging sequences. *American Journal of Neuroradiology*, 27(7), 1459–1462.
- Kerestes, R., Phal, P. M., Steward, C., Moffat, B. A., Salinas, S., Cox, K. L., Ellis, K. A., Cyarto, E. V., Ames, D., Martins, R. N., Masters, C. L., Rowe, C. C., Sharman, M. J., Salvado, O., Szoek, C., Lai, M., Lautenschlager, N. T., & Desmond, P. M. (2015). Alterations in dorsal and ventral posterior cingulate connectivity in APOE ε 4 carriers at risk of Alzheimer's disease. *British Journal of Psychiatry Open*, 1(2), 139–148.
- Kretzschmar, H. A., Ironside, J. W., DeArmond, S. J., & Tateishi, J. (1996). Diagnostic criteria for sporadic Creutzfeldt-Jakob disease. *Archives of Neurology*, 53(9), 913–920.
- Lee, H., Hoffman, C., Kingsley, P. B., Degnan, A., Cohen, O., & Prohovnik, I. (2010). Enhanced detection of diffusion reductions in Creutzfeldt-Jakob disease at a higher B factor. *American Journal of Neuroradiology*, 31(1), 49–54.
- Lee, H., Rosenmann, H., Chapman, J., Kingsley, P. B., Hoffmann, C., Cohen, O. S., Kahana, E., Korczyn, A. D., & Prohovnik, I. (2009). Thalamo-striatal diffusion reductions precede disease onset in prion mutation carriers. *Brain*, 132(Pt 10), 2680–2687.
- Leech, R., Braga, R., & Sharp, D. J. (2012). Echoes of the brain within the posterior cingulate cortex. *Journal of Neuroscience*, 32(1), 215–222.
- Leech, R., & Sharp, D. J. (2014). The role of the posterior cingulate cortex in cognition and disease. *Brain*, 137(1), 12–32.
- Lehmann, M., Madison, C., Ghosh, P. M., Miller, Z. A., Greicius, M. D., Kramer, J. H., Coppola, G., Miller, B. L., Jagust, W. J., Gorno-Tempini, M. L., Seeley, W. W., & Rabinovici, G. D. (2015). Loss of functional connectivity is greater outside the default mode network in non-familial early-onset Alzheimer's disease variants. *Neurobiology of Aging*, 36(10), 2678–2686.
- Lin, Y. R., Young, G. S., Chen, N. K., Dillon, W. P., & Wong, S. (2006). Creutzfeldt-Jakob disease involvement of Rolandic cortex: A quantitative apparent diffusion coefficient evaluation. *American Journal of Neuroradiology*, 27(8), 1755–1759.
- Mahoney, F., & Barthel, D. (1965). Functional evaluation: The Barthel index. *Maryland State Medical Journal*, 14(2), 61–65.
- Manners, D. N., Parchi, P., Tonon, C., Capellari, S., Strammiello, R., Testa, C., Tani, G., Malucelli, E., Spagnolo, C., Cortelli, P., Montagna, P., Lodi, R., & Barbiroli, B. (2009). Pathologic correlates of diffusion MRI changes in Creutzfeldt-Jakob disease. *Neurology*, 72(16), 1425–1431.
- Margulies, D. S., Vincent, J. L., Kelly, C., Lohmann, G., Uddin, L. Q., Biswal, B. B., Villringer, A., Castellanos, F. X., Milham, M. P., & Petrides, M. (2009). Precuneus shares intrinsic functional architecture in humans and monkeys. *Proceedings of the National Academy of Sciences of the United States of America*, 106(47), 20069–20074.
- Mead, S., Ranopa, M., Gopalakrishnan, G. S., Thompson, A. G. B., Rudge, P., Wroe, S., Kennedy, A., Hudson, F., MacKay, A., Darbyshire, J. H., Collinge, J., & Walker, A. S. (2011). PRION-1 scales analysis supports use of functional outcome measures in prion disease. *Neurology*, 77(18), 1674–1683.
- Meissner, B., Kallenberg, K., Sanchez-Juan, P., Collie, D., Summers, D. M., Almonti, S., Collins, S. J., Smith, P., Cras, P., Jansen, G. H., Brandel, J. P., Coulthart, M. B., Roberts, H., Van Everbroeck, B., Galanaud, D., Mellina, V., Will, R. G., & Zerr, I. (2009). MRI lesion profiles in sporadic Creutzfeldt-Jakob disease. *Neurology*, 72(23), 1994–2001.
- Murata, T., Shiga, Y., Higano, S., Takahashi, S., & Mugikura, S. (2002). Concavity and evolution of lesions in Creutzfeldt-Jakob disease at

- diffusion-weighted imaging. *American Journal of Neuroradiology*, 23, 1164–1172.
- Nestor, P., Altomare, D., Festari, C., Drzezga, A., Rivolta, J., Walker, Z., Bouwman, F., Orini, S., Law, I., Agosta, F., Arbizu, J., Nobili, F., & Frisoni, G. B. (2018). Clinical utility of FDG-PET for the differential diagnosis among the main forms of dementia. *European Journal of Nuclear Medicine and Molecular Imaging*, 45, 1509–1525.
- Parchi, P., Giese, A., Capellari, S., Brown, P., Schulz-Schaeffer, W., Windl, O., Zerr, I., Budka, H., Kopp, N., Piccardo, P., Poser, S., Rojiani, a., Streichemberger, N., Julien, J., Vital, C., Ghetti, B., Gambetti, P., & Kretschmar, H. (1999). Classification of sporadic Creutzfeldt-Jakob disease based on molecular and phenotypic analysis of 300 subjects. *Annals of Neurology*, 46(2), 224–233.
- Parchi, P., Strammiello, R., Giese, A., & Kretschmar, H. (2011). Phenotypic variability of sporadic human prion disease and its molecular basis: Past, present, and future. *Acta Neuropathologica*, 121(1), 91–112.
- Pascuzzo, R., Oxtoby, N. P., Young, A. L., Blevins, J., Castelli, G., Garbarino, S., Cohen, M. L., Schonberger, L. B., Gambetti, P., Appleby, B. S., Alexander, D. C., & Bizzi, A. (2020). Prion propagation estimated from brain diffusion MRI is subtype dependent in sporadic Creutzfeldt-Jakob disease. *Acta Neuropathologica*, 140(2), 169–181.
- Pereira, J. M. S., Acosta-Cabronero, J., Pengas, G., Xiong, L., Nestor, P. J., & Williams, G. B. (2013). VBM with viscous fluid registration of gray matter segments in SPM. *Frontiers in Aging Neuroscience*, 5, 1–9.
- Petrella, J. R., Sheldon, F. C., Prince, S. E., Calhoun, V. D., & Doraiswamy, P. M. (2011). Default mode network connectivity in stable vs progressive mild cognitive impairment. *Neurology*, 76(6), 511–517.
- Pievani, M., Filippini, N., van den Heuvel, M. P., Cappa, S. F., & Frisoni, G. B. (2014). Brain connectivity in neurodegenerative diseases—From phenotype to proteinopathy. *Nature Reviews Neurology*, 10(11), 1–14.
- Pillai, K. C. S. (1955). Some new test criteria in multivariate analysis. *The Annals of Mathematical Statistics*, 26, 117–121.
- Puoti, G., Giaccone, G., Rossi, G., Canciani, B., Bugiani, O., & Tagliavini, F. (1999). Sporadic Creutzfeldt-Jakob disease: Co-occurrence of different types of PrP(Sc) in the same brain. *Neurology*, 53(9), 2173–2176.
- Raj, A., Kuceyeski, A., & Weiner, M. (2012). A network diffusion model of disease progression in dementia. *Neuron*, 73(6), 1204–1215.
- Sacco, S., Paoletti, M., Staffaroni, A. M., Kang, H., Rojas, J., Marx, G., Goh, S., Luisa Mandelli, M., Allen, I. E., Kramer, J. H., Bastianello, S., Henry, R. G., Rosen, H. J., Caverzasi, E., & Geschwind, M. D. (2020). Multimodal MRI staging for tracking progression and clinical-imaging correlation in sporadic Creutzfeldt-Jakob disease. *NeuroImage: Clinical*, 30, 102523.
- Sanders, D. W., Kaufman, S. K., Holmes, B. B., & Diamond, M. I. (2016). Prions and protein assemblies that convey biological information in health and disease. *Neuron*, 89(3), 433–448.
- Satterthwaite, T. D., Elliott, M. A., Gerraty, R. T., Ruparel, K., Loughhead, J., Calkins, M. E., Eickhoff, S. B., Hakonarson, H., Gur, R. C., Gur, R. E., & Wolf, D. H. (2013). An improved framework for confound regression and filtering for control of motion artifact in the preprocessing of resting-state functional connectivity data. *NeuroImage*, 64, 240–256.
- Schmahmann, J. D., Doyon, J., McDonald, D., Holmes, C., Lavoie, K., Hurwitz, A. S., Kabani, N., Toga, A., Evans, A., & Petrides, M. (1999). Three-Dimensional MRI Atlas of the Human Cerebellum in Proportional Stereotaxic Space. *NeuroImage*, 10(3), 233–260. <https://doi.org/10.1006/nimg.1999.0459>
- Scott, J. R., Davies, D., & Fraser, H. (1992). Scrapie in the central nervous system: Neuroanatomical spread of infection and Sinc control of pathogenesis. *Journal of General Virology*, 73(7), 1637–1644.
- Seeley, W. W., Crawford, R. K., Zhou, J., Miller, B. L., & Greicius, M. D. (2009). Neurodegenerative diseases target large-scale human brain networks. *Neuron*, 62(1), 42–52.
- Shiga, Y., Miyazawa, K., & Sato, S. (2004). Diffusion-weighted MRI abnormalities as an early diagnostic marker for Creutzfeldt-Jakob disease. *Neurology*, 63, 443–449.
- Staffaroni, A. M., Elahi, F. M., McDermott, D., Marton, K., Karageorgiou, E., Sacco, S., Paoletti, M., Caverzasi, E., Hess, C. P., Rosen, H. J., & Geschwind, M. D. (2017). Neuroimaging in dementia. *Seminars in Neurology*, 37(5), 510–537.
- Stopschinski, B. E., & Diamond, M. I. (2017). The prion model for progression and diversity of neurodegenerative diseases. *The Lancet Neurology*, 16(4), 323–332.
- Tschampa, H. J., Herms, J. W., Schulz-Schaeffer, W. J., Maruschak, B., Windl, O., Jastrow, U., Zerr, I., Steinhoff, B. J., Poser, S., & Kretschmar, H. A. (2002). Clinical findings in sporadic Creutzfeldt-Jakob disease correlate with thalamic pathology. *Brain*, 125(11), 2558–2566. <https://doi.org/10.1093/brain/awf253>
- Tschampa, H. J., Kallenberg, K., Kretschmar, H. A., Meissner, B., Knauth, M., Urbach, H., & Zerr, I. (2007). Pattern of cortical changes in sporadic Creutzfeldt-Jakob disease. *American Journal of Neuroradiology*, 28(6), 1114–1118.
- Tschampa, H. J., Mürtz, P., Flacke, S., Paus, S., Schild, H. H., & Urbach, H. (2003). Thalamic involvement in sporadic Creutzfeldt-Jakob disease: A diffusion-weighted MR imaging study. *American Journal of Neuroradiology*, 24(5), 908–915.
- Ukisu, R., Kushihashi, T., Kitanosono, T., Fujisawa, H., Takenaka, H., Ohgiya, Y., Gokan, T., & Munechika, H. (2005). Serial diffusion-weighted MRI of Creutzfeldt-Jakob disease. *American Journal of Roentgenology*, 184(2), 560–566.
- Vitali, P., MacCagnano, E., Caverzasi, E., Henry, R. G., Haman, A., Torres-Chae, C., Johnson, D. Y., Miller, B. L., & Geschwind, M. D. (2011). Diffusion-weighted MRI hyperintensity patterns differentiate CJD from other rapid dementias. *Neurology*, 76(20), 1711–1719.
- Wang, L. H., Bucelli, R. C., Patrick, E., Rajderkar, D., Alvarez Iii, E., Lim, M. M., Debruin, G., Sharma, V., Dahiya, S., Schmidt, R. E., Benzinger, T. S., Ward, B. A., & Ances, B. M. (2013). Role of magnetic resonance imaging, cerebrospinal fluid, and electroencephalogram in diagnosis of sporadic Creutzfeldt-Jakob disease. *Journal of Neurology*, 260(2), 498–506.
- Watts, J. C., & Prusiner, S. B. (2014). Mouse models for studying the formation and propagation of prions. *Journal of Biological Chemistry*, 289(29), 19841–19849.
- Whitfield-Gabrieli, S., Thermenos, H. W., Milanovic, S., Tsuang, M. T., Faraone, S. V., McCarley, R. W., Shenton, M. E., Green, A. I., Nieto-Castanon, A., LaViolette, P., Wojcik, J., Gabrieli, J. D. E., & Seidman, L. J. (2009). Hyperactivity and hyperconnectivity of the default network in schizophrenia and in first-degree relatives of persons with schizophrenia. *Proceedings of the National Academy of Sciences of the United States of America*, 106(4), 1279–1284.
- WHO. (1998). *Global surveillance, diagnosis and therapy of human transmissible spongiform encephalopathies: Report of a WHO consultation Geneva, Switzerland 9–11 February 1998. World Health Organization: emerging and other communicable diseases, surveillance.* <https://apps.who.int/iris/handle/10665/65516>
- Wu, T., Wang, L., Chen, Y., Zhao, C., Li, K., & Chan, P. (2009). Changes of functional connectivity of the motor network in the resting state in Parkinson's disease. *Neuroscience Letters*, 460(1), 6–10.
- Yeo, B. T. T., Krienen, F. M., Sepulcre, J., Sabuncu, M. R., Lashkari, D., Hollinshead, M., Roffman, J. L., Smoller, J. W., Zöllei, L., Polimeni, J. R., Fischl, B., Liu, H., & Buckner, R. L. (2011). The organization of the human cerebral cortex estimated by intrinsic functional connectivity. *Journal of Neurophysiology*, 106, 1125–1165.
- Younes, K., Rojas, J. C., Wolf, A., Sheng-Yang, G. M., Paoletti, M., Toller, G., Caverzasi, E., Luisa Mandelli, M., Illán-Gala, I., Kramer, J. H., Cobigo, Y., Miller, B. L., Rosen, H. J., & Geschwind, M. D. (2021). Selective vulnerability to atrophy in

- sporadic Creutzfeldt-Jakob disease. *Annals of Clinical and Translational Neurology*, 8(6), 1183–1199.
- Young, G. S., Geschwind, M. D., Fischbein, N. J., Martindale, J. L., Henry, R. G., Liu, S., Lu, Y., Wong, S., Liu, H., Miller, B. L., & Dillon, W. P. (2005). Diffusion-weighted and fluid-attenuated inversion recovery imaging in Creutzfeldt-Jakob disease: High sensitivity and specificity for diagnosis. *American Journal of Neuroradiology*, 26(6), 1551–1562.
- Zerr, I., Kallenberg, K., Summers, D. M., Romero, C., Taratuto, A., Heinemann, U., Breithaupt, M., Vargas, D., Meissner, B., Ladogana, A., Schuur, M., Haik, S., Collins, S. J., Jansen, G. H., Stokin, G. B., Pimentel, J., Hewer, E., Collie, D., Smith, P., ... Sanchez-Juan, P. (2009). Updated clinical diagnostic criteria for sporadic Creutzfeldt-Jakob disease. *Brain*, 132(10), 2659–2668.
- Zhou, F., Gong, H., Li, F., Zhuang, Y., Zang, Y., Xu, R., & Wang, Z. (2013). Altered motor network functional connectivity in amyotrophic lateral sclerosis: A resting-state functional magnetic resonance imaging study. *Neuroreport*, 24(12), 657–662.
- Zhou, J., Gennatas, E. D., Kramer, J. H., Miller, B. L., Seeley, W. W., Raj, A., Kuceyeski, A., & Weiner, M. (2012). Predicting regional neurodegeneration from the healthy brain functional connectome. *Neuron*, 73, 1204–1215. <https://doi.org/10.1016/j.neuron.2011.12.040>
- Zhou, J., Greicius, M. D., Gennatas, E. D., Growdon, M. E., Jang, J. Y., Rabinovici, G. D., Kramer, J. H., Weiner, M., Miller, B. L., & Seeley, W. W. (2010). Divergent network connectivity changes in behavioural variant frontotemporal dementia and Alzheimer's disease. *Brain*, 133(5), 1352–1367.

SUPPORTING INFORMATION

Additional supporting information may be found in the online version of the article at the publisher's website.

How to cite this article: Paoletti, M., Caverzasi, E., Mandelli, M. L., Brown, J. A., Henry, R. G., Miller, B. L., Rosen, H. J., DeArmond, S. J., Bastianello, S., Seeley, W. W., & Geschwind, M. D. (2022). Default Mode Network quantitative diffusion and resting-state functional magnetic resonance imaging correlates in sporadic Creutzfeldt-Jakob disease. *Human Brain Mapping*, 43(13), 4158–4173. <https://doi.org/10.1002/hbm.25945>